Supplementary Information (SI) for Journal of Materials Chemistry B.

Immobilization of iridium nanoparticles on ITO substrate for selective transformation of glycerol to 1, 3-dihydroxyacetone and process tracking

Lin Zhou, Zhanghong Guo, Haining Cui, Jinxin Ma, Chan Wang and Qijun Song

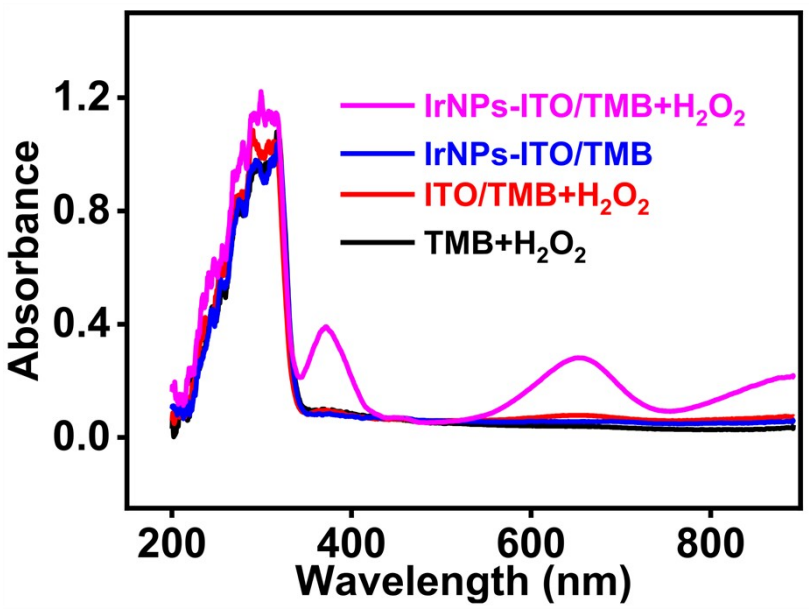

Fig. S1. UV-vis absorption spectra obtained from the catalytic oxidation of TMB by H_2O_2 in the presence of IrNPs-ITO plate, ITO and no catalyst.

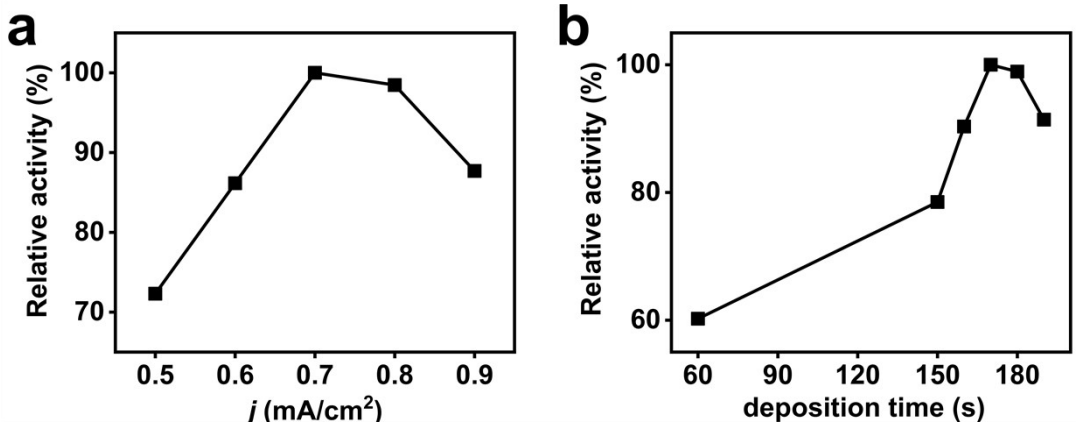

Fig. S2. Plots of (a) the deposition current density and (b) time versus the activity of as-synthesized IrNPs-ITO at 0.5 M K_2SO_4 electrolytes.

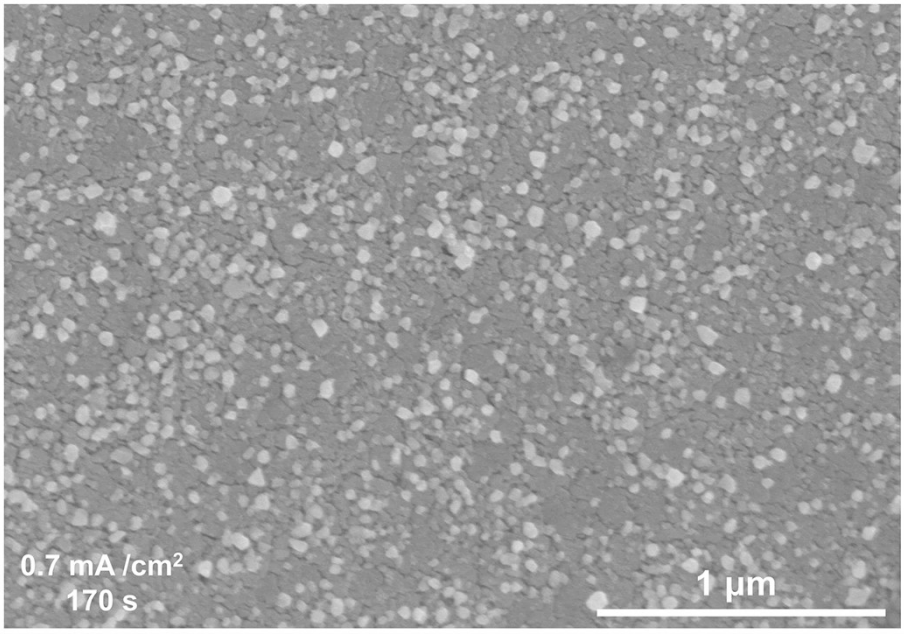

Fig. S3. The SEM image of IrNPs-ITO prepared at 0.5 M K_2SO_4 electrolytes (0.7 mA/cm^2 and 170 s).

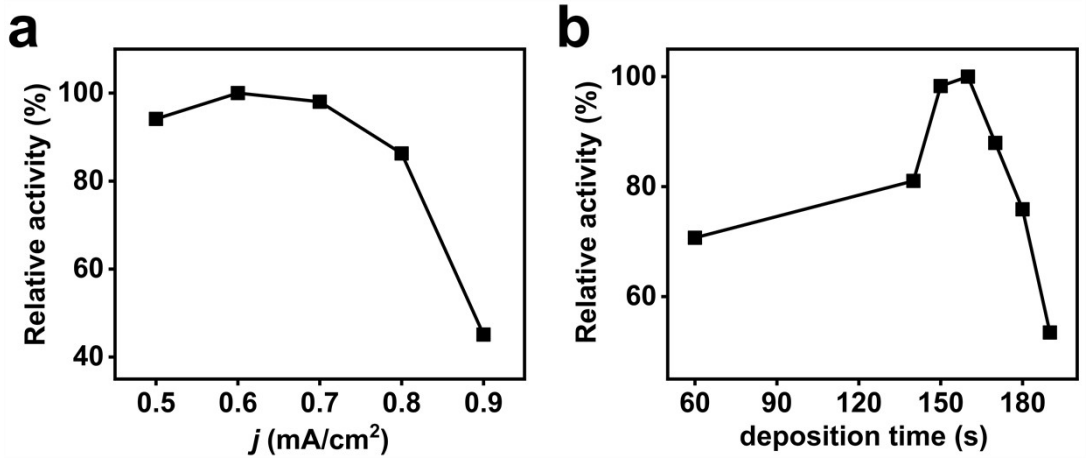

Fig. S4. Plots of (a) the deposition current density and (b) time versus the activity of as-synthesized IrNPs-ITO at 0.5 M KOH electrolytes.

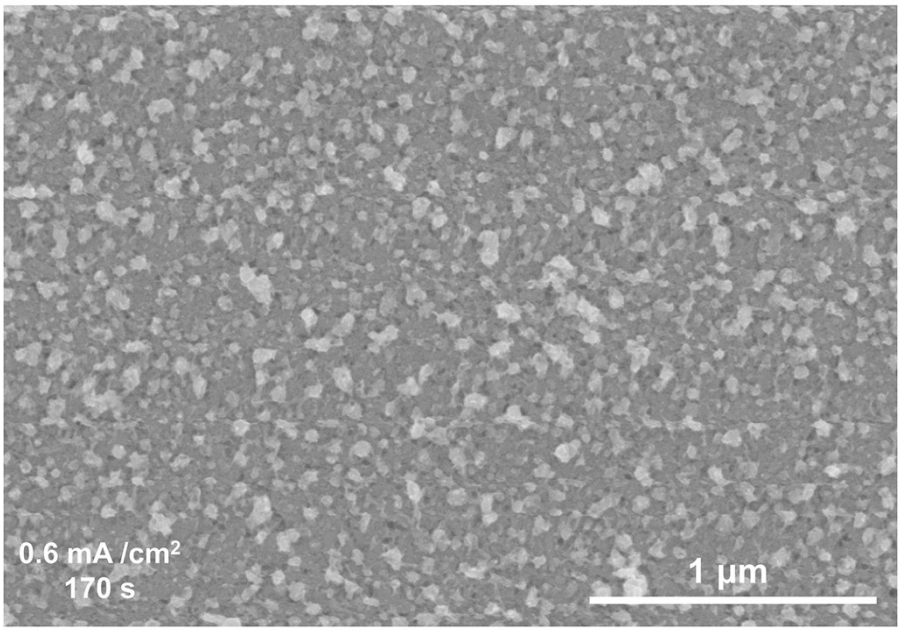

Fig. S5. The SEM image of IrNPs-ITO prepared at 0.5 M KOH electrolytes (0.6 mA/cm^2 and 170 s).

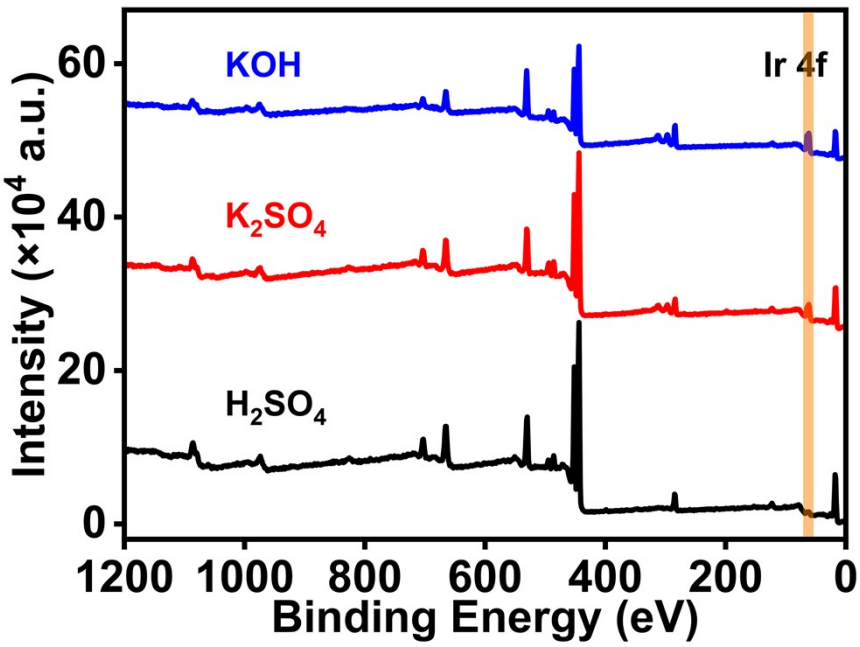

Fig. S6. The full XPS spectra of IrNPs-ITO prepared at different electrolytes.

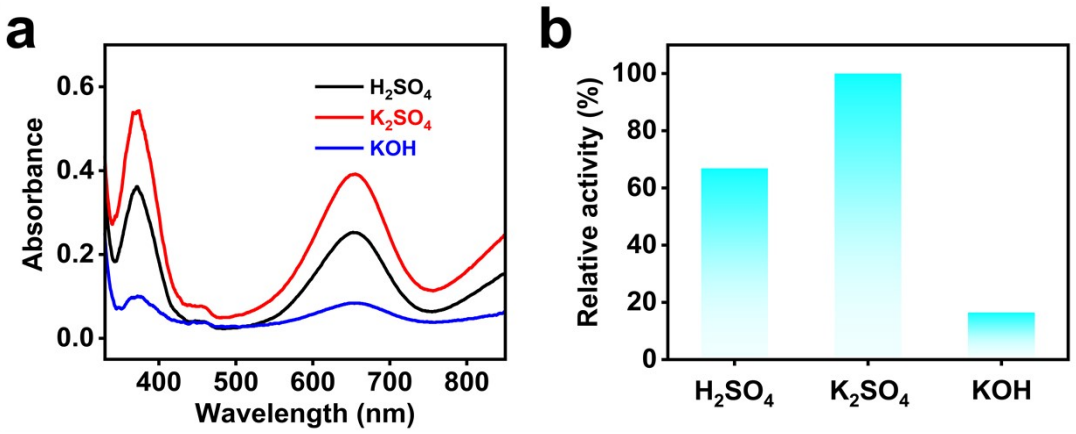

Fig. S7. Comparison of the activities of as-synthesized IrNPs-ITO at different electrolytes: H_2SO_4, K_2SO_4 and KOH (TMB and H_2O_2 as substrates).

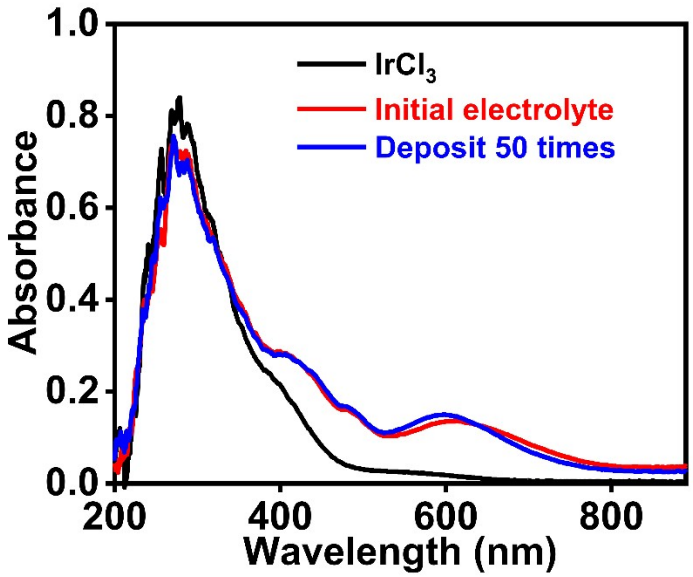

Fig. 8. The UV-vis absorption spectra of the $IrCl_3$ solution and the $IrCl_3$ electrolyte before and after electrodeposition

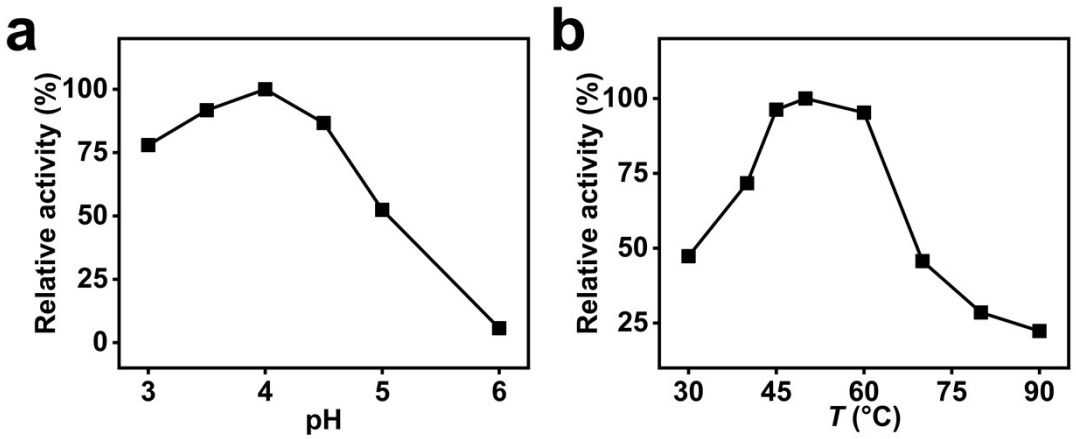

Fig. S9. The effect of (a) pH and (b) temperature on the POD-like activity of the IrNPs-ITO.

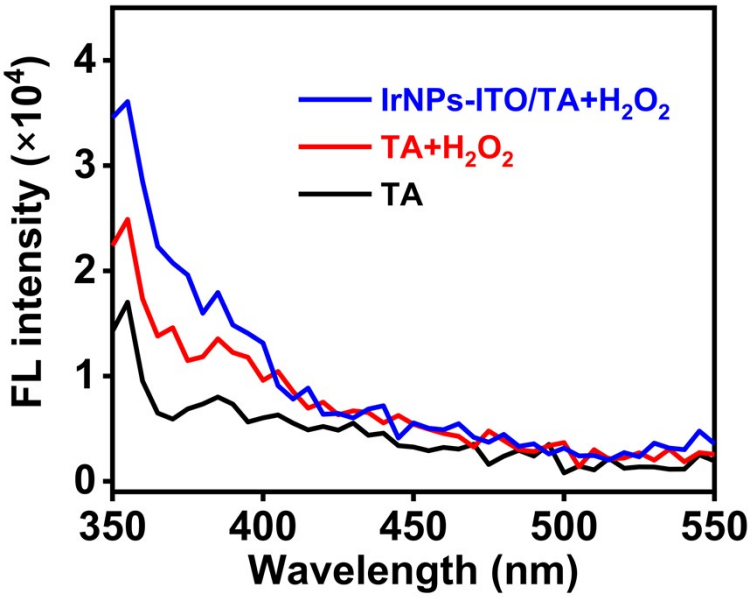

Fig. S10. Fluorescence spectra of reaction solutions containing fluorescent probe TPA with or without IrNPs-ITO.

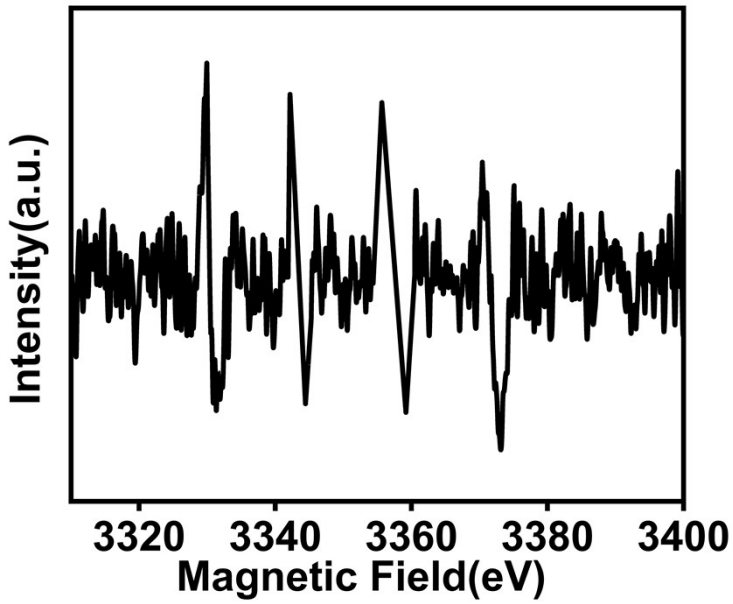

Fig. S11. ESR spectrum obtained from the reaction of DMPO, TMB and H_2O_2 catalyzed by IrNPs-ITO.

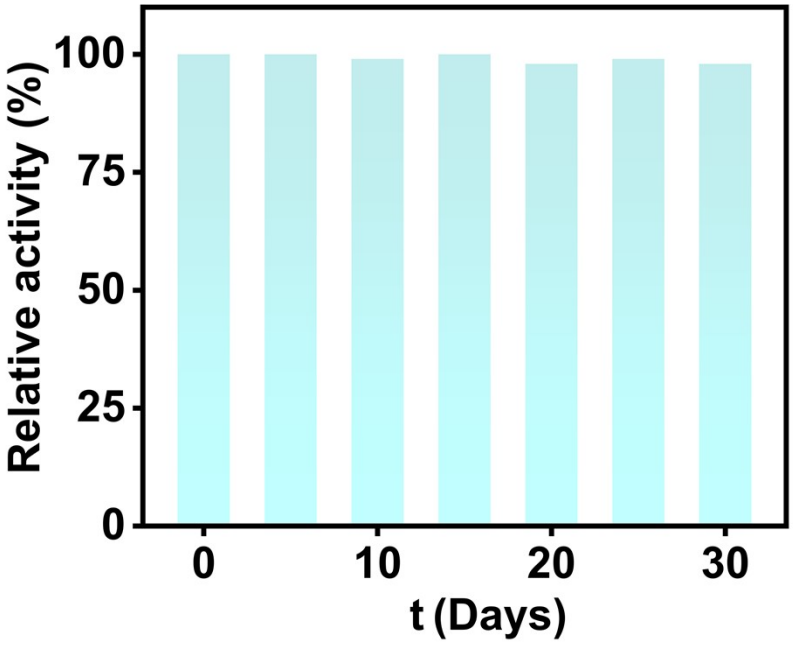

Fig. S12. Stability test of the IrNPs-ITO plate.

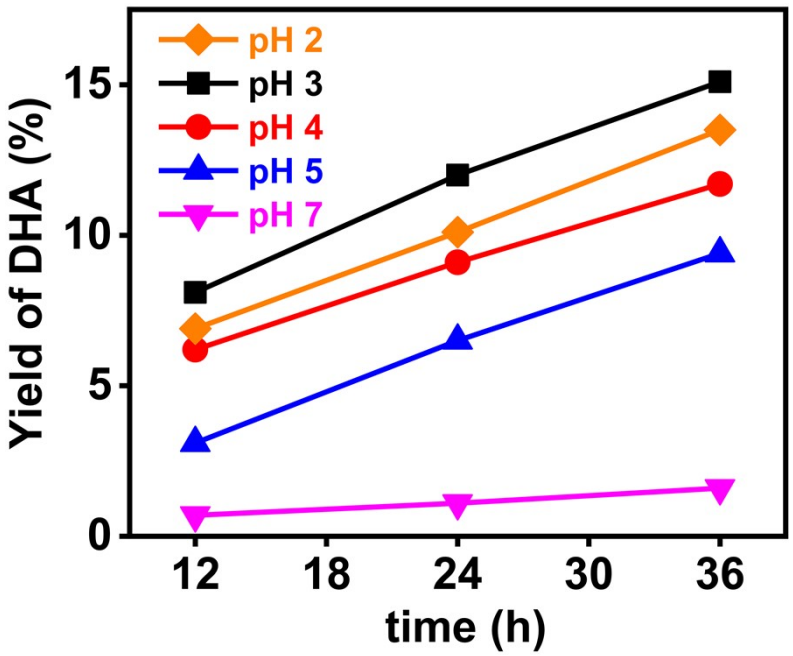

Fig. S13. The effect of pH to the DHA yield.

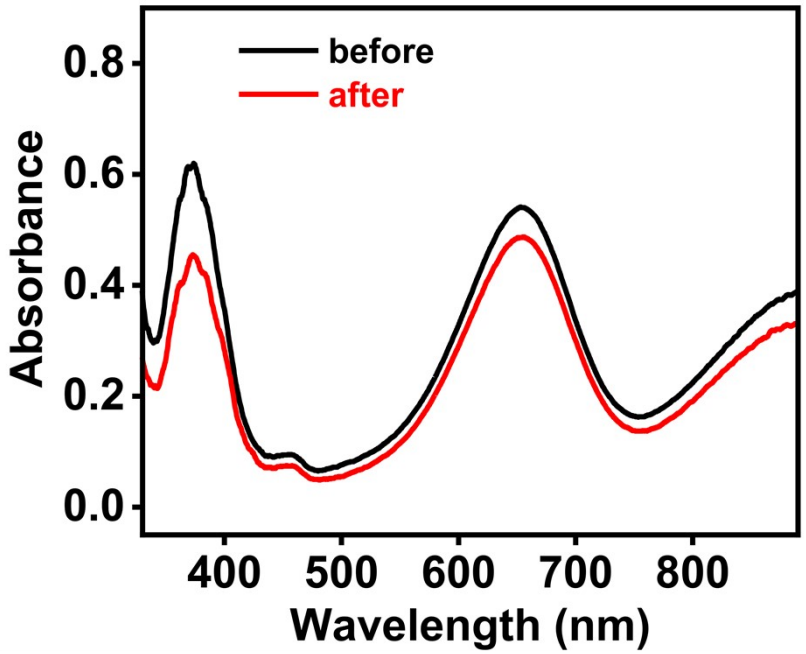

Fig. S14. UV-vis absorption spectrum of the TMB reaction system catalyzed by reused IrNPs-ITO.

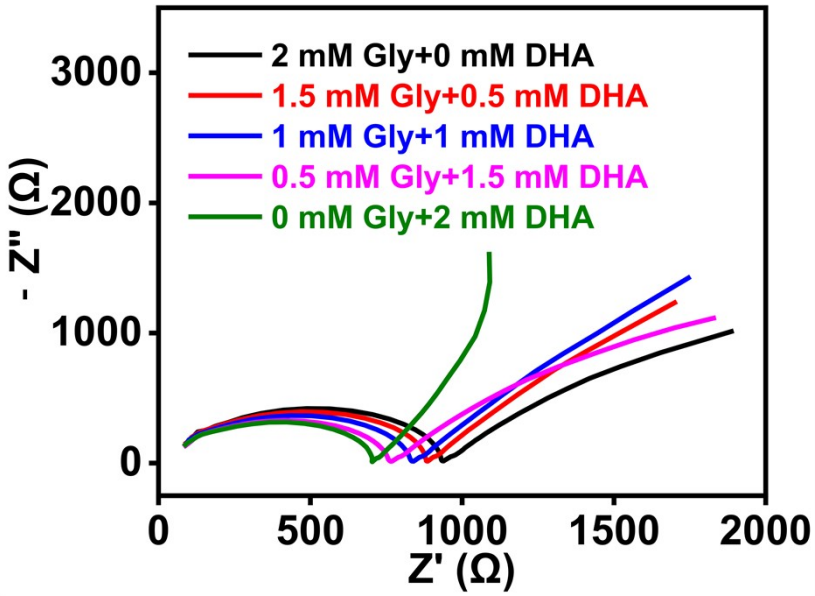

Fig. S15. EIS spectra of solutions containing different DHA concentrations.

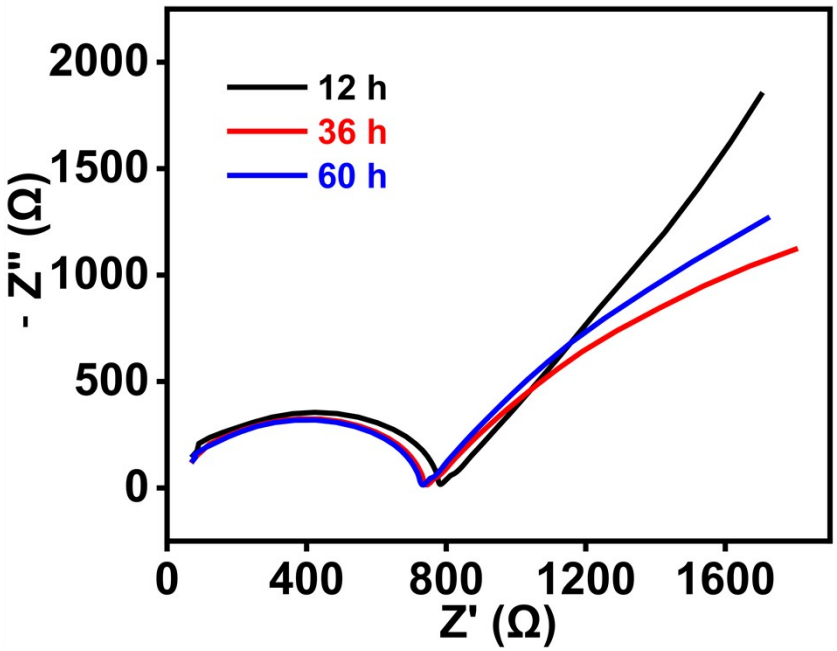

Fig. S16. The impedance chromatograms obtained during the catalytic oxidation of Gly by IrNPs-ITO at different reaction time.

Table S1. Comparison of the kinetic parameters.

	K_m (mM)		v_m (10^{-4} Mm/s)		References
	TMB	H_2O_2	TMB	H_2O_2	
IrNPs-ITO	**0.44**	**0.45**	**0.97**	**1.02**	**This work**
Pt_1/PA	0.17	33	1.13	1.25	[1]
m-MEA	0.82	293	0.27	0.45	[2]
Pt-CS NPs	0.28	1.42	1.97	3.87	[3]
Pt SAN	0.21	0.21	1.8	3.2	[4]
Pt_{NPs}/Pt_{SA}-NC-800	0.37	20.72	0.84	0.38	[5]

Table 2. Comparison of the catalytic oxidation performance of Gly.

Catalyst	Reaction conditions	DHA		Ref.
		Selectivity (%)	Yield (%)	
ITO-IrO_2	**H_2O_2, 90 °C, 60 h, 0.5 mM H_2SO_4**	**~87.0**	**~87.0**	**This work**
Au/ZnO-RF	O_2, 1 MPa; 100 °C, 1 h	76.2	69.4	[6]
$Au/Cu_{0.9}Zn_{0.1}$	O_2, 0.2 MPa; 50 °C, 4 h	93.2	70.0	[7]
Au/ZnO-D	O_2, 1 MPa; 60 °C, 4 h	69.0	37.3	[8]
$Au/CuZnO_x$@bZ	O_2, 1 MPa; 80 °C, 2 h	86.0	80.0	[9]
S3-Au/CuO	O_2, 1 MPa; 100 °C, 2 h	82.0	71.0	[10]
Au_2Cu_1/ZnO	O_2, 1.5 MPa; 60 °C, 5 h	83.4	75.6	[11]
P-doped Pd/CNT	0.5 M KOH, Electro-oxidation	90.82	/	[12]
Pt/C electrode in Bi-sat	0.5 M H_2SO_4, Electro-oxidation	100	/	[13]

Table S3. Comparison of impedance obtained with different working electrodes at the start and end of the reaction. Error bars represent the standard errors derived from three repeated measurements.

	IrNPs-ITO	ITO
Aqueous solution (pH 3)	768.43 ± 51.63 Ω	795.33 ± 54.06 Ω
2 mM Gly solution (pH 3)	887.97 ± 68.76 Ω	812.98 ± 61.73 Ω
30 mM H_2O_2 solution (pH 3)	733.59 ± 59.49 Ω	696.60 ± 56.82 Ω
2 mM Gly and 30 mM H_2O_2 solutions (pH 3)	848.38 ± 69.20 Ω	774.20 ± 51.86 Ω
2 mM DHA solution (pH 3)	621.88 ± 59.81 Ω	658.13 ± 36.36 Ω

References

[1] Q. Liu, G. Li, Y. Cao, Y. Ren, Q. Qin, L. Li, H. Zhang, Q. Xin, X. Gong, L. Zhao, S. Zhang, Y. Li, J. Yang, J. Zhang, X. Mu, X. Zhang. Single-atom nanozyme immunoassay with electron-rich property for clinical patient cancer detection. *Chem. Eng. J.* **2025**, *506*, 159940.

[2] Y. Zhang, Y. Kang, X. Wei, C. Chen, Y. Zhai, C. Zhu, L. Jiao, X. Lu, Y. Yamauchi.

Modulating *p-d* orbital hybridization in mesoporous medium-entropy alloy nanozymes with enhanced peroxidase-like activity. *ACS Nano* **2025** 19, 24013–24022.

[3] L. Dang, A. Zhang, J. Li, J. Cao, X. Rong, M. Su, B. Du, Y. Bu. ATP-enhanced platinum nanoparticle's peroxidase activity in alkaline environment for simplifying alkaline phosphatase detection. *Sens. Bio-Sens. Res.* **2025**, *48*, 100798.

[4] Z. Lin, G. Sun, H. Liu, X. Zhang, Z. Bian, A. Liu. Mechanism of pesticide thiram reversibly inhibiting of Pt single-atom peroxidase-mimicking nanozyme and its application in colorimetric sensing thiram. *Talanta* **2025**, *294*, 128201.

[5] S. Liu, Z. Liu, L. Chen, R. Li, X. Liu, X. Jia. Pt nanoparticles modified single-atoms nanozymes with tunable metal valence for rapid chlorpyrifos colorimetric

detection. *Biosens. Bioelectron.* **2025**, *287*, 117730.

[6] X. Zhang, H. Liu, Y. Ke, W. Xie, J. Huang, Y. Chen, Z. Xiong, Z. Yuan. Biomimetic flower-petal-architected Zn-based nanocatalysts for selective oxidation of glycerol to 1, 3-dihydroxyacetone. *ACS Appl. Nano Mater.* **2025**, *8*, 14052–14064.

[7] Y. Wang, W. Liu, J. Zhao, Z. Wang, N. Zhao. Oxidation of glycerol to dihydroxyacetone over highly stable Au catalysts supported on mineral-derived CuO-ZnO mixed oxide. *Appl. Catal. A-Gen.* **2024**, *671*, 119578.

[8] H. Yan, M. Zhao, Y. Cao, X. Zhou, Y. Liu, X. Chen, X. Feng, X. Duan, F. Zaera, X. Zhou, C. Yang. Crystal-facet-dependent, electron sink effect for the enhanced selective oxidation of polyols at the secondary hydroxyl position. *J. Catal.* **2024**, *431*, 115401.

[9] Z. Yuan, Y. Wang, W. Xie, Y. Chen, X. Zhang, X. Zhang, Z. Xiong, L. Cui, H. Liu. Manipulating the interfacial integration mode of a bio-templated porous ZSM-5 platform with an Au/CuZnO_x catalyst for enhanced efficiency and recycling stability in glycerol conversion to 1,3-dihydroxyacetone. *Nanoscale* **2025**, *17*, 5259–5269.

[10] L. Cui, F. Wang, X. Zhang, Y. Chen, H. Liu, Y. Ke, Y. Wang, X. Zhang. Plant-mediated biosynthesized Au/CuO catalysts for efficient glycerol oxidation to 1,3-dihydroxyacetone: effect of biomass component on catalytic activity. *New J. Chem.* **2024**, *48*, 19206–19219.

[11] M. Zhao, H. Yan, R. Lu, Y. Liu, X. Zhou, X. Chen, X. Feng, H. Duan, C. Yang. Insight into the selective oxidation mechanism of glycerol to 1,3-dihydroxyacetone over AuCu-ZnO interface. *AIChE J.* **2022**, *68*, e17833.

[12] M. Ahmad, S. Singh, C. Cheng, H. Ong, H. Abdullah, M. Khan, S. Wongsakulphasatch. Glycerol electro-oxidation to dihydroxyacetone on phosphorous-doped Pd/CNT nanoparticles in alkaline medium. *Catal. Commun.* **2020**, *139*, 105964.

[13] Y. Kwon, Y. Birdja, I. Spanos, P. Rodriguez, M. Koper. Highly selective electro-oxidation of glycerol to dihydroxyacetone on platinum in the presence of bismuth. *ACS Catal.* **2012**, *2*, 759-764.